Morphotectonic and morphometric analysis of the Nazca plate and the adjacent offshore Peruvian continental slope – implications for submarine landscape evolution

Nina Kukowski[1*], Andrea Hampel[2], Silvan Hoth[3], Jörg Bialas[4]

[1]GeoForschungsZentrum Potsdam, Telegrafenberg, 14473 Potsdam, Germany; Tel.: +49 (0) 331 288 1318, Fax: +49 (0) 331 288 1370; e-mail: Nina.Kukowski@gfz-potsdam.de

[2]Institut für Geologie, Mineralogie und Geophysik, Gebäude NA, Raum 2/163, Ruhr-Universität Bochum, Universitätsstr. 150, 44801 Bochum, Germany; Tel.: +49 (0) 234 32 27718, Fax: +49 (0) 234 32 14572, e-mail: andrea.hampel@ruhr-uni-bochum.de

[3]GeoForschungsZentrum Potsdam, Telegrafenberg, 14473 Potsdam, Germany; Tel.: +49 (0) 331 288 1306, Fax: +49 (0) 331 288 1370; e-mail: shoth@gfz-potsdam.de

[4]Leibniz-Institut für Meereswissenschaften IFM-GEOMAR, Wischhofstr. 1-3, Geb. 8/C-207, 24148 Kiel, Germany; Tel.: +49 (0) 431 600 2329Fax : +49 (0) 431 600 2922, e-mail: jbialas@ifm-geomar.de

*corresponding author

Key-words: swath bathymetry, morphotectonics, morphometry, convergent margins, Peru, submarine slumping, curvature analysis, morphometric dating, submarine landscape evolution, hazard potential

Abstract

We use new swath bathymetry data acquired during the *RV Sonne* cruise GEOPECO and complement them with swath data from adjacent regions to analyse the morphotectonics of the Peruvian convergent margin. The Nazca plate is not covered with sediments and therefore has a rough surface along the entire Peruvian trench. The styles of roughness differ significantly along the margin with linear morphological features trending in various directions, most of them oblique to the trench and roughness magnitudes of a few to several hundred meters. The lower slope is locally very rough and at the verge of failure throughout the entire Peruvian margin, as a result of subduction erosion causing the lower slope to over-steepen. Using curvature attributes to quantitatively examine the morphology in the Yaquina and Mendaña areas revealed that the latter shows a larger local roughness both seaward and landward of the trench. However, the amplitude of morphological roughness is larger in the Yaquina area. We identified a 125 km^2 large slump on the Lima middle slope. Morphometric dating suggests an age of 74500 years within 35 to 40% error. Estimated incision rates on the upper slope are between 0.1 and 0.3 mm per year suggesting that landscape evolution on the Peruvian submarine continental slope is similarly slow than that in the Atacama desert.

1. Introduction

Quantifying variability in continental slope gradient or slump scar gradient as well as a description of local and regional variability of seafloor morphology has only become possible since the late 1970’s when scientific swath mapping campaigns began, and has more frequently been undertaken since the early 1990’s, when a new generation of much more efficient swath mapping systems became available (Bourillet et al., 1996). Unlike onshore morphometry, which has been widely applied employing gridded digital elevation data, marine morphometry is considered to be still in its infancy (e.g. Ramsay et al., 2006). However, although not frequently, high-resolution multibeam swath bathymetry has been used for detailed and quantitative morphotectonic and morphometric analyses (e.g. Huchon and Bourgois, 1990; Duperret et al., 1995; Pratson and Haxby, 1996; von Huene et al., 1999, Kukowski et al., 2001, Sak et al., 2004, Mitchell, 2005) and also revealed its high potential in aiding to assess the hazard potential of a margin (e.g. McAdoo et al., 2004). Morphometric dating of slumps using a diffusion transport model has been suggested to be also applicable in submarine environments (e.g. Mitchell, 1996).

According to the mode of material transfer, convergent margins are divided into accretive and erosive ones and both show a very different morphology. The continental slopes of accretive margins like Cascadia or Makran on a regional scale have a very gently inclined slope of less than 2˚ and are mainly characterized by along-strike elongated topographic ridges forming the surface expression of an accretionary wedge. The large length (up to more than 100 km) of these ridges and the relative morphological smoothness of their flanks, while being relatively steep, suggest that these ridges are quite stable (e.g. Pratson and Haxby, 1996; Kukowski et al., 2001). The continental slopes of those margins undergoing subduction erosion and where therefore a pronounced accretionary wedge is missing, are regionally steeper, and show a more irregular topography suggested to result from distributed surficial mass wasting caused by over-steepening as a result of transferring material from the tip of the slope to the subduction channel (e.g. Ranero and von Huene, 2000; von Huene and Ranero, 2003). Compared to accretive margins, erosive margins like the Peruvian tend to be more prone to the occurrence of major slumps, which have been made responsible for having caused tsunamis with run-up heights up to 50 meters (e.g. von Huene et al., 1989).

The Peruvian convergent margin is a prominent example of a long-term erosive margin (e.g. Karig, 1974, von Huene and Lallemand, 1990, Clift et al., 2003). Here the nearly sediment-free and very rough (Kulm et al., 1973, Huchon and Bourgois, 1990) Nazca plate is obliquely subducted beneath South America. The structure of the margin is well known from reflection seismic (Moore and Taylor, 1988, von Huene et al., 1996), and wide-angle seismic (Hampel et al., 2004, Krabbenhöft et al., 2004) data and parts of the margin have been surveyed with swath mapping and side scan sonar (e.g. Bourgois et al., 1988; Hussong et al., 1988; Huchon and Bourgois, 1990; Li and Clark, 1991; Hagen, 1993; Li, 1995; Bourgois et al., 2007).

In this study we use new swath bathymetry data obtained during the German *RV Sonne* GEOPECO cruise (Bialas and Kukowski, 2000) to analyse the morphology and deformation styles of the Nazca plate approaching the trench and the continental slope along the Peruvian margin (Fig.1). We add SEAPERC swath data (Huchon and Bourgois, 1990) to our data-base to extend the multibeam coverage along the margin. The analysis of the whole dataset includes a quantitative comparison employing curvature attributes for two sub-regions. We also attempt to morphometrically date a newly identified slump on the upper continental slope off Lima. By doing so, we are able to roughly estimate the rates of landscape evolution at the Peruvian continental slope.

2 Geodynamic setting and structure of the Peruvian margin

Along the Peruvian margin (Fig.1), the close to sediment-free oceanic Nazca Plate is subducting in largely easterly direction (N78°E) beneath the South American continent at a present convergence rate of ~68 mm/a (Norabuena et al., 1998) resulting in about 20° obliquity of convergence in recent times. The age of the subducting plate increases from about 28 Ma north of 10°S to about 40 Ma south of

16°S (Fig.1) with a considerable jump in age across the Mendaña Fracture Zone (MFZ) (Müller et al., 1997). The trench is well pronounced and more than 6000 m deep along most of the Peruvian margin. It shallows towards the Nazca Ridge (NR), a prominent, more than 1000 km long basement ridge the crest of which is rising about 1.5 km above the surrounding seafloor. This ridge has swept southwards along the margin since its first collision at about 11°S some 10 Myr ago to 15°S where it presently subducts beneath the Peruvian margin (Hampel, 2002, Rosenbaum et al., 2005).

Close to the trench, the descending Nazca plate dips between 5.5° and 9° and the average dip of the lower continental slope varies regionally between 7° and 9° (Krabbenhöft et al., 2004, Hampel et al., 2004). Juxtaposed to the trench is a small low-velocity accretionary wedge of less than 20 km width throughout the margin and landward of it follows high-velocity continental basement most probably of Palaeozoic age (von Huene et al., 1996, Krabbenhöft et al., 2004). Along the upper slope with a thick Quaternary sediment cover, several elongated forearc basins, e.g. the Talara, Yaquina, Lima and Pisco Basins, indicate significant Cenozoic subsidence.

Major Quaternary slumping has been reported from several localities along the Peruvian margin. A polyphase large-scale submarine slump between 5°S and 6°S dated at 13.8 ± 2.7 ka (von Huene et al., 1989; Bourgois et al., 1993; Duperret et al., 1995) and a giant slump identified at about 20°S (Li and Clark, 1991) are the most prominent evidence for slope instability and related hazard potential.

3. Data acquisition, processing, and analysis

During *RV Sonne* cruise GEOPECO (Bialas and Kukowski, 2000) extensive swath mapping was undertaken in several areas between 8°S and 16°S employing the onboard Hydrosweep system (Grant and Schreiber, 1991). Swath data were acquired to cover certain areas (Fig.1) as well as when doing seismic profiling and transits.

The individual beams of a swath are often of different quality. Whereas beams close to the centre of a swath hit the seafloor at a right angle and usually are of high quality, the beams at the edges of a swath hit the seafloor at low angles which may lead to a lower quality. In order to obtain a high quality swath map, it is necessaryto place ship tracks sufficiently close to obtain some overlap between neighbouring swaths. This was done in the Yaquina area and along the lower continental slope, and we therefore obtained full coverage in these areas. Ship's speed was less than 10 knots while mapping, and 4 to 5 knots during seismic work. We added further individual swaths obtained e.g. during wide angle seismic work (Hampel et al., 2004; Krabbenhöft et al., 2004) to our data set. Spatial resolution along a swath is about 200 m in water depths as deep as the trench and 70 meters and higher in water shallower than 2000 meters, respectively. Along track, the spacing of swaths was some 10s of meters according to the ship's speed.

Each swath was edited using the freely available MB system software package (Caress and Chayes, 1995) for visual inspection of the data quality. The latter was generally high, due to the calm weather during the entire cruise. Non-frequent erroneous outer beams were removed from the data set. After editing, the raw data were converted to depth using a water sonic velocity profile obtained from a CTD (conductivity-temperature-depth tool) at a trench-near position (Bialas and Kukowski, 2000). Vertical accuracy of the depth-converted data is ± 2 meters. Geographical coordinates were assigned to each beam using the ship's navigation. In a final step, data were re-formatted to 3 column ascii data to generate various sub-grids for morphotectonic and morphometric analysis.

For this study, we also used swath bathymetry data obtained during *RV Jean Charcot* SEAPERC cruise in 1986 (Bourgois et al., 1988), which we received as 3 column ascii data. We did not apply any further processing to this data set, as it was used in several studies before (e.g. Bourgois et al., 1988; Huchon and Bourgois, 1990; Duperret et al., 1995). Merging the GEOPECO and SEAPERC data revealed a very good fit in the (small) overlapping regions confirming the good quality and reliability of these data sets. In the Lima region, we digitized ODP bathymetry and added it to our data to enable a more regional picture. The swath data were complemented with GINA (Lindquist et al., 2004) data for some analyses to characterize the regional seafloor morphology across the edges of the areas covered with swath bathymetry. However, all our interpretations have been exclusively derived from the high-resolution swath data. Sub-grids and profiles were extracted from the whole data set for detailed analysis and to display maps and perspective views.

A straight-forward strategy to quantitatively analyse a digital terrain model, such as a gridded swath bathymetry data set is to compute the local dip for each cell, allowing to e.g. identify areas potentially close to failure (e.g. McAdoo et al., 2004) or quantifying the morphological roughness (also called ruggedness) of an area. However, many morphological features have a linear trend, which cannot be identified from the dip alone. Here, curvature attributes computed from gridded curved surfaces, e.g. gridded topographic data (Shary et al., 2004) or seismic horizons mapped from 3D reflection seismic data sets (Roberts, 2001) are an efficient tool to support tectonic interpretation and detect features such as faults or quantify local dip. Surface curvature attributes describe how much a surface deviates from a plane and also may characterize the cause of this deviation (Roberts, 2001; Bergbauer & Pollard, 2003). Mathematically curvature is defined as the 2^{nd} derivative of a curve. With this definition, a dipping, but straight line has a zero curvature, while a non-straight line has a non-zero curvature. The basic definition of curvature in two dimensions also holds for three dimensions, i.e. for a curved surface. With this definition, for any given point on a curved plane an infinite number of curvatures can be extracted, as the cut can be made in any direction. However, those curvatures defined by planes orthogonal to the surface are most useful for structural analysis (Roberts, 2001). There will be one curve with the largest curvature. Perpendicular to it is the curve with the smallest curvature. This maximum and minimum curvatures then are used to derive further curvature attributes, but also can be directly used e.g. to delimit faults and fractures. Curvature extracted in the direction of maximum dip allows to measure the rate of change of dip. In this dip curvature (profile curvature in terrain analysis; Shary et al., 2004) the direction of faults is preserved and therefore contains information complementary to that derived from local dip.

To compute curvature attributes of gridded bathymetry surfaces we employed a least square quadratic approximation fitting a local surface by using the neighbouring eight grid values which results in a set of arithmetic expressions for the coefficients of the quadratic polynom describing the surface (Roberts, 2001). Grid cell size was carefully chosen in accordance with the spacing of the GEOPECO swath bathymetry data, as a proper choice of grid cell size may be crucial for a sound interpretation (Bergbauer & Pollard 2003). As curvature analysis is quite sensitive to filters applied, we used unfiltered grids to avoid bias of the analysis. We extracted subsets of the bathymetry data to analyse the nature of the Nazca plate approaching the trench and the lower slope in two areas, the Yaquina area off Trujillo and the area of the MFZ.

A slump scar or a fault scar is steepest just after failure and re-adjusts through superficial erosion to the average regional slope angle with time. For transport limited systems, like at continental slopes, this process of degradation can be approximated with a diffusion process (Coleman and Watson, 1983; Mitchell, 1996) and therefore can be described by the diffusion equation

$\partial z / \partial t = dc (\partial^2 z / \partial x^2)$,
where z is elevation, t is time, dc is the diffusion coefficient and x is the horizontal distance. The faster a slump scar degrades to the regional slope, the larger is the diffusion coefficient. Analytical and numerical solutions for the diffusion equation have been proposed yielding the product of the diffusion coefficient and the age of the slump or faulting event (e.g. Nash, 1981; Coleman and Watson, 1983; Mitchell, 1996). This means that the equation is underdetermined as long as both, the diffusion coefficient and the age of a slump are not known. However, it enables to date a slump morphometrically relative to a slump in the same setting, which has been dated using other techniques, e.g. isotopic methods. The analytical solution of Coleman and Watson (1983) offers the possibility to date a slump without knowing the slope of the escarpment just after failure. However, this method has been debated, because it suggests that the degradation is dependent on the height of the scarp, and because it does not account for sedimentation but it offers to date a slump without knowing the slope gradient just after failure. Otherwise, plausible estimates need to be made for the slope gradient just after faulting or slumping, e.g. assuming a vertical scarp or the angle of repose.

4. Morphological characteristics of the Peruvian slope and facing Nazca plate

In the following description and quantitative analysis of the swath bathymetry data we focus on two key-areas (Yaquina and MFZ) seaward of the trench where full coverage allows to quantitatively analyse the surface of the Nazca plate. Further, the new bathymetry data enable to visualize the morphology of the lower slope continuously along about 400 km along the margin. In the Lima region, full coverage was achieved on the middle and parts of the upper and lower slopes, respectively. Here, we were able to identify a major slump and estimate its age using the above mentioned diffusion law based morphometry and comparison with a well-known (Bourgois et al., 1993; Duperret et al., 1995) slump further to the north in the Paita area.

4.1 Morphology of the Nazca plate approaching the Peruvian margin

Generally, the surface of the Nazca plate seaward of the Peru trench is close to sediment-free (http://www.ngdc.noaa.gov/mgg/sedthick/sedthick.html). In the absence of sediment coverage, original surface roughness, i.e. as generated at the spreading centre, will be maintained on old oceanic crust (Bird and Pockalny, 1994). Therefore, at sediment-starved margins like the Peruvian one the morphology of the oceanic crust at the trench still mimics the processes and directions of its generation.
The main regional topographic feature of the Nazca plate close to the Peru trench is a ripple pattern made of elongated highs and lows oriented at different angles to the trench with a spacing of a few kilometres and a height difference of about 100 to a few hundreds of meters (Figs.2, 3). Seaward of Trujillo trough and the northern Lima trench, this pattern is similar in shape and height magnitude to that found on young (0 to 10 Ma) Nazca plate crust not far away from the East Pacific Rise (Grevemeyer et al., 2002). Although the depth of the trench changes along the Peruvian margin, the regional bend of the Nazca plate towards the trench is similar along the entire margin with the seafloor 50 km seaward of the trench being approximately 1.3 to 1.4 km shallower than the trench (Fig.3). The only exception is Nazca ridge, where the Nazca plate is bending considerably steeper.

4.1.1. Yaquina area

Between 7.5º S, the latitude, at which Trujillo Trough intersects with the trench, and the northern edge of the Mendaña Fracture zone the Nazca plate seafloor shows some unique features. Between 8º S and

8.65º S, five parallel, ridge-shaped features trending grossly parallel to the convergence direction (N78E), enter the trench (Fig.4). At the seaward trench wall, some of them are cut by bending-related normal faults. We interpret them as relicts of former transform faults, which are now healed. A half-moon shaped re-entrant on the lower continental slope facing one of these “ridges” at 8.25° S is similar to re-entrants formed in the wake of subducting seamounts (e.g. Dominguez et al., 1997) indicating that this “ridge” has already been subducting some distance beneath the lower slope. South of 8.65°S, several roughly north-south trending ridges of about 35 km length enter the trench. These basalt ridges are oblique to any other feature, including the direction of convergence. The direction of their long axes is at angles of 14° to 24° relative to the trench (Fig.2a). We interpret them to result from off-axis magmatism and having remained in their original direction and shape when approaching the trench. These ridges mark the largest local scale roughness of the Nazca plate with the height difference between the top of the basalt ridges and the surrounding seafloor being as large as more than 800 m at some locations (Fig.2, 3, 4).

4.1.2 Mendaña Fracture Zone

Morphologically, the MFZ is a sequence of elongated features trending perpendicular to the trench (Fig.5). Its width is at least 80 km. In the north, the elongated features resemble ridges being parallel to each other and south of 10.5° S, the morphology shows several stair case like steps which are dipping to the SE. The width of both the ridges and the steps is about 10 to 15 km and their surfaces are generally very rough. The difference in elevation between adjacent ridges and troughs on average is several hundred meters and up to 600 m at maximum. The flanks to the troughs, which are mostly characterized by rough surfaces, are steeply dipping. This pattern is well compatible with differential vertical motion along numerous parallel sub-vertical faults indicating extension in N-S direction (Fig.5). Bending related normal faults cannot be clearly identified, however, the irregular surface of the ridges and troughs and the partially bad swath coverage may obscure such features. The ridges and steps maintain their shapes when entering the trench and are cut off along a straight line (Fig.5). There are no re-entrants or other morphological features indicating their subduction at the tip of the lower continental slope. Either these features are too small to influence the lower slope morphology in a characteristic manner or they have just arrived at the trench. Off Yaquina, only the most pronounced ridge (3 in Fig.4) created a re-entrant. This ridge however is wider and higher than the other ridges off Yaquina and those forming the MFZ. This would suggest that the MFZ is already subducting beneath the Peruvian slope, but a feature too smooth to significantly affect the lower slope morphology.

To compare Nazca plate as well as the trench and its both sides quantitatively, we applied curvature analysis to the Yaquina region (Fig.6) and the MFZ (Fig.7) and also present histograms showing the distribution of local dip in the two areas, seaward and landward of the trench, respectively (Fig.8). The ripple-topography on the Nazca plate facing the Yaquina slope is characterized by walls of about 10º dip on average with portions of the flanks being as steep as 15º to 20º (Fig. 6b). Between the ripples, the seafloor is close to flat and the “regional” roughness does not increase towards the trench. We could not identify bending related normal faults in this part of the Nazca plate. The N-S-trending scarp at 81.05º W (see black arrows in fig.6a) is as steep as at least 15º throughout its entire length. The basalt ridges in the trench have steep flanks and relatively flat tops with NW-SE-trending structures, similar to those just west of the N-S-scarp (Fig.4, 6a). The immediate proximity of negative and positive values of dip curvature confirms the sudden change of morphology along the basalt ridges (see black arrows in Fig.6c) and suggests to interpret the scarp at the tip of the western flank of the westernmost ridge as a fault scarp.

A much larger portion of the MFZ surface has a steepness of more than 5° compared to the Yaquina trench region (Fig.8). Between 80.4° W and 80.2°W, a roughly N-S oriented linear trend cuts through the entire length of the area displayed (black arrows in Fig.7b, c). The direction of this trend is at high angle to the ship's course and therefore cannot be an artefact. We suggest it to be the surface expression of a fault, probably a strike-slip fault with a normal component. This structure is difficult to identify from just the topographic map (Fig.5, 7a). Here, like for the trench-perpendicular normal faults, the immediate proximity of positive and negative dip-curvature values (red arrows in Fig.7b, c) confirms that these structures may be interpreted as faults.

4.1.3 Lima area

At 11.75º S, ripple-shaped structures on the Nazca plate are parallel to the trench (Fig.2b), whereas at 13.5ºS they strike more southerly generating about 10º obliquity (Fig.2c) between the ripples and the trench. A comparison with the area in-between (Gagnon et al., 2004) reveals that the trend of these morphological features changes at 12.5º S. The spacing between neighbouring peaks is approximately 5 to 10 km. In profile view, at 13.5º S, the morphology of the seaward wall of the trench looks like tilted steps with seaward slopes more shallowly dipping than landward slopes. The ripple-shaped morphology with an elevation amplitude of a few hundred meters is a regional pattern seaward of the Peruvian trench with the Yaquina region and the MFZ being pronounced exceptions. The ripples do not have the same trend everywhere, which we interpret in accordance with Grevemeyer et al. (2002) to be related to the different spreading directions when the Nazca plate crust was formed.

4.2 Trench and continental slope

Bathymetry profiles across the trench and continental slope at different latitudes (Fig.3) reveal a lower slope with a similar large steepness of about 6º along the entire margin. Between 8°S and 11°S, the lower slope is characterized by a rough and irregular morphology (Figs.4, 5) consisting of equi-dimensional and elongated highs and lows, and also local ruggedness of the seafloor. This very much resembles the morphology of the lower slope in the Paita area as described by Bourgois et al. (1988). In agreement with these authors we interpret this morphology to results from local mass wasting. The tip of the continental slope is not a straight line along the trench, but it locally advances and recedes in an alternate way. This was named a meandering front by Huchon and Bourgois (1990), who describe this type of deformation front in the Mendaña area. The new GEOPECO data reveal that this type of deformation front continues at least as far north as 8°S.

Structural benches of some 10 to 30 km length are present on the continental slope throughout the entire margin, however, their width and relative height are very variable (e.g. Schweller et al., 1981). Several terraces and elongated ridges are regional marks in the morphology of the lower slope (Figs.4, 5). In the north, these features look more like narrow terraces, in the south more like peaked ridges. Especially the ridges found along the lower slope facing the MFZ (Fig.5b) very much resemble accretionary ridges found at margins like the Makran (Kukowski et al., 2001) or Cascadia (Pratson and Haxby, 1996). Accordingly,we interpret them as accretionary ridges as well.

In the Yaquina area, the lower slope is characterized by two irregular bands of high steepness, which locally can attain 30º indicating that large portions of the lower slope may be at the verge of failure. The trench is not marked by a straight line, but as a sequence of advancing and retreating segments (red arrows in Fig.6b). We interpret the advancing portions as originating from local slope failure.

This is very nicely seen in the display of dip-curvature (Fig.6c). Landward adjacent to the lower slope is a narrow, but relatively flat mid-slope terrace. There, a patchy band made up of discontinuous very narrow ridges (see blue arrows in Fig.6c) marks the surface expression of a fault, which we interpret to be a continuation of a normal fault identified further to the south earlier (Bourgois et al., 1988). Dip curvature (Fig.6c) reveals the higher linearity and continuity of the slope benches compared to the fault zone itself, which creates a patchy image, and the middle slope which exhibits irregular local-scale topography.

The tip of the upper slope roughly coincides with 3000m water depth and is characterized by the presence of numerous, grossly equally spaced mostly v-shaped gullies (Fig.9). This observation reveals that here surface morphology could develop which has resulted from self-organisation (Hampton et al., 1996). During the incision of these gullies, the upper Peruvian slope must have been stable. The profiles across the upper slope show a significant ruggedness and irregularity of the topography. However, the main gullies are still very prominent. Furthermore, the main gullies straightly follow the dip of the slope and all of them are fed by numerous smaller feeder gullies creating a dendritic pattern also observed at passive margins (Pratson and Haxby, 1996; Goff, 2001). The gullies frequently are more than hundred meters deep, the main gullies even as deep as about 200 m. The average gradient of the upper slope is about 5º, which makes it close as steep as the lower slope. In contrast to the latter it must be relatively stable since it is underlain by Palaeozoic metamorphic continental basement. A possible reason for the higher stability of the upper slope is that it consists of intact rock, which exhibits a high cohesion.

The lower slope in the MFZ area very much resembles the one of the Yaquina region, portions of it are even steeper and the ridges are more discontinuous. The landward edge of the lower slope is marked by a patchy, relatively flat area of considerable width, very different from what is observed in the Yaquina region. Not only does the MFZ region exhibit a larger percentage of local dips of more than 5º and even 20º compared to the Yaquina off-trench region, but the same is observed at the continental slopes (Fig.8). Especially the Mendaña continental slope is characterized by non-Gaussian distribution of dip. The frequency distribution of local dip of both portions of the continental slope off Peru analysed here is dissimilar to the one documented along the convergent accretive Oregon continental slope (Pratson and Haxby, 1996). At the Peruvian margin, local slope gradients are significantly less frequent and steep slope gradients are more frequent than at the Cascadia margin, with the regional slope gradient being twice as high. This may imply that convergent margins undergoing subduction erosion form their own class with regard to local slope. Also the regional slope of the Peruvian margin seems to be significantly steeper than those of the other types of margins, confirming this suggestion.

4.3 Surficial mass wasting and catastrophic mass transport

Local surficial mass wasting is expressed in various ways along the central Andean submarine slope. Local, but steady redistribution of material is characteristic for the lower slope in the Yaquina and Mendaña regions (see 4.2), but also at the NR collision zone (Hampel et al., 2004). This implies that the entire Peruvian margin may be characterised by this locally rugged lower slope. However, the middle and upper slopes in these regions show different characteristics. The absence of gullies suggests that the upper slope in the Mendaña region also is close to failure. In addition, at about 10.5ºS, we identified a large slump mass at the tip of the upper slope (Fig. 5b).

The morphology of the Lima area in some aspects differs from the other parts of the Peruvian margin. It has a wide mid-slope terrace and the surface of it is smoother than north of it. In the swilley south of the Northern High (Pecher et al., 2001), a large meandering channel with tributary channel systems is identified (Fig.10). In analogy to the term river drainage basin used for onshore runoff systems we call it a turbidity current basin. The development of this channel system suggests a relatively long-term stability of the mid-slope. From visual inspection, sub-basins do not mimic the basin itself, therefore they are not self-similar (Dodds and Rothman, 2000).

Between 11.2ºS and 11.4ºS, a large slump mass covering an area of about 125 km^2 and having a relatively steep seaward rim is identified from the swath data (Fig.10). Bathymetry profiles through the escarpment and the slump mass (Fig.11) reveal a thickness of 200 m and volume of 40 km^3 of the slump mass. The toe of the slump escarpment is half-moon-shaped and the surface of the escarpment comprises numerous gullies indicating that the slump must be old enough such that a drainage system could evolve.

Both the slump off Paita and the Lima slump occurred on the middle slope between 3000 m and 4000 m water depth (Fig.11a,b), which may suggest that similar rocks occur beneath the slumps scarps. Also, the escarpments of both slumps have approximately the same height (Fig.11c, d), which justifies to normalize the analytical solution of Coleman and Watson (1983). Therefore, comparing both slump scars morphometrically allows for a cautious estimation of the age of the Lima slump by using the steepness of the escarpments and the far-field slopes, respectively (Fig.11b). The average slopes across the escarpments and the far-field slopes are estimated graphically (Fig.11c, d). The average slope of the Paita escarpment is as steep as 17° with a far-field slope in this portion of the Peruvian mid-slope of about 5.7°. As its age is known, we estimated a diffusion coefficient of 0.0026 m^2/yr for the Paita slump, assuming the initial slump scarp was sub-vertical, as observed from the N-S profile across the slump scarp. The slump scarp may have moved landward with the detachment fault as steep as 45° as reported by Bourgois et al. (1988) on the middle and upper slope, producing a decrease of the relative slope gradient of the scar, from its initial gradient (90°) to the actual one (17°). The average slope of the Lima escarpment is 6.35° and the far-field slope 2.5°.Using the value of the diffusion coefficient obtained for the Paita slump, we estimate the age of the Lima slump at 74520 years. For the age estimate of the Paita slump, an error of 20% was estimated (Bourgois et al., 1993), which then is the minimum error for the age of the Lima slump, as the estimation of its age is based on the estimation of the age of the Paita slump The curved shape of the escarpments and the deviation of the profiles from a straight line add an uncertainty of the estimation of the slope angles of about 1°, which would add an error of 5 to 15 % depending on the actual slope. Since we describe large scarps with a height of several hundred meters and given that bioturbation is usually limited to the uppermost about 50 cm of sediment, we consider it to be of minor importance. This is supported by the observation that not far from the upper edge of the Lima slump, competent rocks are outcropping (Pecher et al., 2001), which do not seem to have been re-worked by bioturbation. Taking all this in account, the error in the estimate of the age of the Lima slump may be as large as 35 to 40 %.

The gullies developed in the Lima slump escarpment reveal that it has been stable since slumping. To assume that incision of the gullies started immediately after slumping enables to roughly estimate incision rates. The gullies are at least as deep as 10 m with a maximum of about 25 m. This would infer incision rates between 0.1 mm and 0.33 mm per year. Taking the potentially large error of the age of the slump into account, incision rates may well vary between 0.07 and 0.5 mm per year.

5. Discussion

The new GEOPECO swath bathymetry data together with older complementary data enables to draw a regional scale picture of the morphological features and their diversity of the Nazca plate and continental margin off Peru. The close to sediment-free Nazca plate exhibits a remarkably high roughness, though expressed in different styles along the Peruvian margin, mostly of higher roughness than e.g. the Nazca plate off north Chile (von Huene and Ranero, 2003) and the Cocos plate off Costa Rica north of Nicoya peninsula (Ranero and von Huene, 2000), respectively. Bending-related normal faults, which are commonly observed on sediment-free oceanic plates close to subduction zone trenches (e.g. Ranero and von Huene, 2000; Wright et al., 2000; Ranero et al., 2005), have been identified in our swath data on the Nazca plate north of 9º S (Fig.4), in the Lima region between 11º and 13.5º S (Fig.2), and in the collision zone of Nazca Ridge at about 15º S (Hampel et al., 2004). Earlier studies in adjacent regions have revealed a consistent picture (Hussong et al., 1988). However, bending-related normal faults are absent between 9º S and 11º S (Fig.4). Note, that for the MFZ, we do not follow the interpretation of Huchon and Bourgois (1990), who reported bending-related normal faults. However, as the SEAPERC data do not provide full coverage (See Fig.1), interpretation of structures parallel to the ship tracks is problematic. These regions correspond with an unusual morphology of high roughness and linear elements with different trends on the Nazca plate suggesting that the direction of lower plate morphological features may suppress the formation of such faults, whereas the amount of bending, or the average slope of the lower plate towards the trench (Fig.3) does not seem to influence the occurrence and spacing of normal faults (Fig.2, 4). The ridges identified in the Yaquina area trench consist of tholeiitic basalt of Miocene age (8.7 Ma, Kulm et al., 1974). Miocene ages, although older, have also been found for basalts (16.5 Ma and 18.6 Ma) in the MFZ (Bourasseau et al., 1993). This is considerable younger than the age of the Nazca plate close to the trench (> 27 Ma, Fig.1) and infers that considerable mid-plate magmatism seems to have occurred in the Miocene.

The trench is about 5 km wide along most of the Peruvian margin and has a flat surface, which is in contrast e.g. to the north Chilean margin (von Huene and Ranero, 2003) that also is shaped by subduction erosion. The toe of the continental slope is not straight but overprinted by ubiquitous local slumps , which is similar to what is observed along the north Chilean margin (von Huene and Ranero, 2003), but different from most accretive margins (e.g. Kukowski et al., 2001, McAdoo et al., 2004). The lower slope up to about 1500 m above the trench is of very similar steepness along the margin, while escarpments on the middle slope become wider and more distinct from north to south (Fig.3). We interpret the “ridges” or “benches” identified on the lower slope (Fig.3, 6, 7) as relicts of accretionary ridges comparable to those at typical accretive margins. However, as sediment input also during accretive phases most probably did not exceed some hundred meters thickness (von Huene et al., 1996), they are quite narrow-spaced and not very pronounced. In this aspect, the Peruvian margin is different from other erosive margins where there is no accretionary prism, but a margin wedge sensu Ranero and von Huene, 2000, e.g. north Chile and Costa Rica.

The similarity of the morphology of the lower slope throughout the whole margin and the highly variable morphology of the lower plate may infer that there is no direct link between them. A possible reason is that the lower slope is at the verge of extensional failure (Davis et al., 1983), caused e.g. by elevated fluid pressure or subduction erosion. High fluid pressure is quite likely close to the trench (Kukowski & Pecher, 1999), reducing the effective strength along the décollement and therefore facilitating extensional failure. The steepness of the lower slope may be caused by frontal subduction erosion (Kukowski and Oncken, 2006), a process, by which material originating from gravitational failure of the lower slope is incorporated in the subduction channel. A rough lower plate favours subduction erosion. Therefore, if lower plate morphology were a factor driving slope instability this would suggest that the roughness of the Nazca plate is sufficient to do so along the entire Peruvian margin. This would imply that, as soon as lower plate roughness is sufficiently high, frontal subduction erosion and gravitational failure of the lower slope occur independent of the specific style of lower plate morphology. As most sediment-free lower plates exhibit a well pronounced surface roughness, if true, this would imply that lower slopes at erosive margins may usually be at or close to the limit of extensional failure.

The differences of both the Nazca plate morphology and the lower slope morphology in the Yaquina and Mendaña areas, respectively, have been quantitatively revealed using curvature attributes. By doing so, we have yield information that can not be extracted from traditional bathymetric maps nor from single beam profiles. As the Nazca plate in the Mendaña region exhibits a higher percentage of steeper areas compared to the Yaquina area, this would suggest e.g. a higher potential impact on frontal subduction erosion. A largely N-S trending fault scar seaward of the trench cutting the MFZ which was not identified from the topographic map, but only from the displayed curvature attributes reveals the high potential of this method to process and interpret swath data.

Between 6º and 20º S, surface mass wasting mainly occurs at a local scale. The slump we identified on the Lima (125 km^2) slope covers an area considerably smaller than the Holocene slumps at 5º S and 20º S, which cover areas as large as 660 km^2 and 2200 km^2. However, the slumps identified off Peru fall in size among the about 20 largest slumps in the entire north Atlantic, which occurred there in a comparable late Pleistocene and Holocene period (Maslin et al., 2004). Slumps comparable in size to that on the Lima slope were also reported in the southern Yaquina area (Bourgois et al., 1988). Common to these slumps off Peru is that they originated along major (normal) faults on the middle slope inferring a close relation with the extensional tectonics originating from over-steepening due to subduction erosion. The Lima slump is located very close to the "Northern High", a structural high, beneath which methane flux rates are quite high such that a BSR could develop in a fast subsiding environment (Pecher et al., 2001). If this slump had tectonic causes, the sudden absence of an 800 m high sediment column would have significantly altered the stability conditions of gas hydrates. However, on the other hand, the long-term stability of the Lima escarpment after slumping might infer that hydrate triggered slumping not necessarily may result in regional scale catastrophic slope failure.

Although it needs several only loosely constrained assumptions and therefore contains a large error, morphometric dating of submarine slumps offers an efficient tool to quantify the rates of submarine landscape development. To our knowledge, the diffusion coefficient of 0.0026 m^2/yr (with 35 to 40% error) obtained from the Paita slump is the first reported from a convergent margin. Having the large error in mind, this value is similar toa small diffusion coefficient of 0.007 m^2/yr obtained for scarp degradation in the Galapagos spreading centre (Mitchell, 1996). This slow degradation after slumping at the Peruvian margin may explain why the Paita slump still looks very fresh and point to relatively slow submarine landscape evolution at this margin.

Assuming that erodibility is largely the same along the Peruvian margin, the incision rates estimated from the gullies in the Lima slump escarpment offer to estimate the age of the gullies at the Yaquina upper slope, some of which are incised as deep as 200 m. If incision rates were between 0.1 and 0.3 mm per year, these gullies developed in 0.6 to 2 Myrs, inferring long-term stable conditions along this portion of the upper submarine slope. Surface erosion in the hyper-arid Central Andes is slow and several authors suggested that the Atacama desert is the oldest onshore landscape on earth (Dunai et al., 2005; Gonzales et al., 2006). Schlunegger et al. (2006) report incision rate of 0.05 to 0.25 mm/yr at 18°S latitude. Also, Schildgen et al. (2007) report incision rates of 0.01 mm per yr during the Cenozoic before 10 Ma, 0.26 mm/yr during late Miocene and 0.5 mm per yr during Pliocene for an onshore canyon running towards the Peruvian coast at 16° S. These onshore rates are very similar to those we obtained from our morphometric analysis for the submarine Peruvian slope. This would imply that landscape evolution in the submarine and onshore Peruvian forearc is taking place at comparable rates. Due to the arid climate prevailing in the Central Andes since the Oligocene (Dunai et al., 2005), erosion in the onshore Central Andean forearc has been very slow throughout this time period and the Peruvian continental slope received only very little terrestrial material. Therefore, the slow rates of submarine landscape evolution may be a direct consequence of the slow rates of onshore landscape evolution.

6. Conclusions

The new swath bathymetry data and complementary data presented in this paper allow to draw a regional scale picture of the morphological diversity of the Nazca plate seaward of the Peru trench and the Peruvian continental slope. We used morphometric analyses and curvature analyses more extensively than done in previous studies. Such tools enable more quantitative information extracted from swath bathymetry data in addition to displaying maps and their structural interpretation.

Several morphological features contribute to the large roughness of the surface of the Nazca plate: the ripple morphology with an amplitude up to a few hundred meters as the most typical type of seafloor morphology, palaeo-transform faults, basalt ridges with steep flanks and elevated as much as up to 800 m above the surrounding seafloor, and narrow ridges making up the MFZ in a horst-and-graben sequence.

Bending-related normal faulting is widely present seaward of the Peru trench, but absent between 9 and 11 °S, which coincides with the very unusual morphology of the Nazca plate in the Yaquina region.

The roughness of the Nazca plate decreases towards the south. The lower slope generally is very unstable, whereas the upper slope is relatively stable with downslope transport taking place through equi-spaced gullies. A comparison between the Yaquina and Mendaña regions reveal the large roughness of the Nazca plate and the lower slope in both regions, but local steepness generally is larger in the Mendaña region, whereas the magnitude of roughness is higher in the Yaquina region.

There is ample evidence for local failure due to over-steepened slopes. The local scale ruggedness and failure of the lower slope is characteristic for the entire Peruvian margin and therefore most probably linked to subduction erosion.

We identified a 125 km^2 large slump on the Lima middle slope. Comparison with a large slump off Paita the age of which is known, allowed to morphometrically estimate the age of the Lima slump to be 74.5 ka with an about 35 to 40% error. Scarp diffusion with a diffusion coefficient of 0.0026 m^2/yr and incision rates of 0.1 to 0.3 mm/yr are quite slow at the Peruvian margin, making rates of gully incision and landscape evolution similar to those in the Atacama desert, which is regarded as the slowest evolving onshore landscape.

The present study emphasises the usefulness of morphological and morphometric analyses in aiding our understanding of hazard generation, especially for tsunamis and landslides. It also confirms that a detailed knowledge of morphology which can only achieved by swath mapping is essential to understand the rates and styles of submarine landscape evolution.

Acknowledgements

The GEOPECO Project has been funded by the German Ministry of Education and Research (BMBF). We thank Cpt. Papenhagen and his crew for excellent support during the cruise. We acknowledge J. Bourgois for making the SEAPERC bathymetry data available to us. The GINA (Lindquist, 2004) data set has been used to complement topographic data in regions without swath covering. Maps and diagrams were produced with the GMT software (Wessel and Smith, 1998). We thank two anonymous reviewers and the editor D. J. W. Piper for their detailed comments.

References

Bergbauer, S., Pollard, D.D., 2003. How to calculate normal curvatures of sampled geological surfaces. J. Struct. Geol. 25, 277 – 289.

Bialas, J., Kukowski, N. (eds.), 2000. Cruise Report SO 146 GEOPECO, GEOMAR Report 96, 490pp.

Bird, R.P., Pockalny, R.A., 1994. Late Cretaceous and Cenozoic seafloor and oceanic basement roughness: Spreading rate, crustal age, and sediment thickness correlations. Earth Planet. Sci. Lett. 123, 239 – 254.

Bourasseau I., Juteau T., Karpoff, A.-M., Bourgois, J., Bellon., H., 1993. Exploration des structures volcaniques de la ride d'accrétion de Mendaña au large du Pérou: resultats de la campagne Nautiperc du submersible *Nautile*, avril 1991. C. R. Acad. Sci. Paris, t.317, Série II, 1097 – 1103.

Bourgois, J., Pautot, G., Bandy, W., Boinet, T., Chotin, P., Huchon, P., Mercier de Lepinay, B., Monge, F., Monlau, J., Pelletier, B., Sosson, M., von Huene, R., 1988. Seabeam and seismic reflection imaging of the tectonic regime of the Andean contientnal margin off Peru (4°S to 10°S). Earth Planet. Sci. Lett. 87, 111 – 126.

Bourgois, J., Lagabrielle, Y., De Wever, P., Suess, E., NAUTIPERC Team, 1993. Tectonic history of the northern Peru convergent margin during the past 400 ka. Geology 21, 531 – 534.

Bourgois, J., Bigot-Cormier, F., Bourles, D., Braucher, R., Dauteuil, O,. Witt, C., Michaud, F., 2007. Tectonic record of strain buildup and abrupt co-seismic stress release across the northwestern Peru coastal plain, shelf, and continental slope during the past 200 kyr. J. Geophys. Res. 112, B04104, doi:10.1029/2006JB004491.

Bourillet, J.F., Edy, C., Rambert, F., Satra, C., Loubrieu, B., 1996. Swath mapping system processing: bathymetry and cartography. Mar. Geophys. Res. 18, 487 – 506.

Caress, D.W., Chayes, D.N., 1995. New software for processing sidescan data form sidescan-capable multibeam sonars. In: Proceedings of the IEEE Ocean 95 Conference pp. 997 – 1000, Mar. Technol.Soc., Washington DC

Clift, P.D., Pecher, I.A., Kukowski, N., Hampel, A., 2003. Tectonic erosion of the Peruvian forearc, Lima Basin, by steady-state subduction and Nazca Ridge collision. Tectonics 22/3, 1023, doi:10.1029/2002TC001386.

Coleman, S.M., Watson, K., 1983. Ages estimated from a diffusion equation model for scarp degradation. Science 221, 263 – 265.

Davis, D., Suppe, J., Dahlen, F.A., 1983. Mechanics of fold-and-thrust belts and accretionary wedges. J. Geophys. Res. 88, 1153-1172.

Divins, D.L., NGDC Total Sediment Thickness of the World's Oceans & Marginal Seas, Retrieved date goes here, *http://www.ngdc.noaa.gov/mgg/sedthick/sedthick.html*

Dodds, P.S., Rothman, D.H., 2000. Scaling, universality, and geomorphology. Annu. Rev. Earth Planet. Sci 28, 571 – 610.

Dominguez, S., Lallemand, S.E., Malavieille, J., von Huene, R., 1998. Upper plate deformation associated with seamount subduction. Tectonophysics 293, 207 – 224.

Dunai, T., Gonzales, G., Juez-Larré, J., 2005. Oligocene-Miocene age of aridity in the Atacama Desert revealed by exposure dating of erosion-sensitive landforms. Geology 33, 321 – 324, doi:10.1130/G21184.1.

Duperret, A., Bourgois, J., Lagabrielle, Y., Suess, E., 1995. Slope instabilities at an active continental margin: large-scale polyphase submarine slides along the northern Peruvian margin, between 5°S and 6°S Mar. Geol. 122, 303 – 328.

Gagnon, K., Chadwell, C.D., Norabuena, E., 2005. Measuring the onset of locking in the Peru-Chile trench with GPS and acoustic measurements. Nature 437, 205 – 208.

Goff, J.A., 2001. Quantitative classification of canyon systems on continental slopes and a possible relationship to slope curvature. Geophys. Res. Letters 28, 4359 – 4362.

Gonzales, G., Dunai, T., Carrizo, D., Allmendinger, R., 2006. Young displacement on the Atacama fault system, northern Chile from field observations and cosmogenic ^{21}Ne concentrations. Tectonics 25, TC3006, doi:10.1029/2005TC001846.

Grant, J.A. and Schreiber, R., 1990. Modern swath sounding and sub-bottom profiling technology for research applications: The Atlas Hydrosweep and Parasound systems. Mar. Geophys. Res. 12, 9 -19.

Grevemeyer, I., Schramm, B., Devey, C.W., Wilson, D.S., Jochum, B., Hauschild, J., Aric, K., Villinger, H.W., Weigel, W., 2002. A multibeam-sonar, magnetic and geochemical flowline survey at 14° 14'S on the southern East Pacific Rise: insights into the fourth dimension of ridge crest segmentation. Earth Planet. Sci. Lett. 1999, 359 – 372.

Hagen, R.A., 1993. Fault patterns on the outer wall of the Peru-Chile trench. Geo-Mar. Lett. 13, 139 – 144.

Hampel, A., 2002. The migration history of the Nazca Ridge along the Peruvian active margin: a re-evaluation. Earth Planet. Sci. Lett. 203, 665 – 679.

Hampel, A., Kukowski, N., Bialas, J., Hübscher, C., Heinbockel, R., 2004. Ridge subduction at an erosive margin - the collision zone of the Nazca Ridge in southern Peru. J. Geophys. Res. 109, B02101, doi:10.1029/2003JB002593.

Hampton, M.A., Lee, H.J., Locat, J., 1996. Submarine Landslides. Rev. Geophys. 31, 33 – 59.

Huchon, P., Bourgois, J., 1990. Subduction-induced fragmentation of the Nazca plate off Peru: Mendaña fracture zone and Trujillo trough revisited. J. Geophys. Res. 95, 8419 – 8436.

Husson, D.M., Reed, T.B., Bartlett, W.A., 1988. SEAMARC II sonar imagery and bathymetry of the Nazca plate and Peru forearc, ODP Leg 112. In: Suess E, von Huene R et al., Proc. ODP, Init Rept. 112, 125 – 130.

Karig, D.E., 1974. Tectonic erosion at trenches. Earth Planet. Sci. Lett. 21, 209 – 212

Krabbenhöft, A., Bialas, J., Kopp, H., Kukowski, N., Hübscher, C., 2004. Crustal structure of the Peruvian continental margin from wide-angle seismic studies. Geophys. J. Int. 159, 749 – 964, doi:10.1111/j1365-246X.2004.02425.x.

Kukowski, N., Schillhorn, T., Huhn, K., von Rad, U., Flueh, E.R., Husen, S., 2001. The Makran accretionary wedge: morphotectonic analysis, erosive canyons, and implications for forearc mechanics. Mar. Geol. 173, 1-19.

Kukowski, N., Oncken, O., 2006. Subduction erosion – is this the "normal" mode of fore-arc material transfer along the Chilean margin? In: Oncken O, Strecker M, Franz G, Ramos V (eds) Andean Geodynamcs, Frontiers in Geosciences 1, Springer, 217 – 236.

Kulm, L.D., Scheidegger, K.F., Prince, R.A., Dymond, J., Moore, T.C., 1973. Tholeiitic basalt ridge in the Peru trench. Geology 1, 11 – 14.

Li, C., 1995. Forearc structures and tectonics in the southern Peru – Northern Chile continental margin. Mar. Geophys. Res. 17, 97 – 113.

Li, C., Clark, A.L., 1991. SEAMARC II study of a giant submarine slump on the northern Chile continental slope. Mar. Geotechnology 10, 257 – 268.

Lindquist, K.G., 2004. Global topography and bathymetry grid improves research efforts. EOS Trans. AGU, 85 (19): 186-187.

Maslin, M., Mikkelsen, N., Vilela, C., Haq, B., 1998. Sea-level- and gas hydrate controlled catastrophic sediment failures of the Amazon Fan. Geology 1998, 1107 – 1110.

McAdoo, B.G., Capone, M.K., Minder, J., 2004. Seafloor geomorphology of convergent margins: Implications for Cascadia seismic hazard. Tectonics 23, doi:10.1029/2003TC001570.

Mitchell, N.C., 2005. Interpreting long-profiles of canyons in the USA Atlantic continental slope. Mar. Geol. 214, 75 – 99.

Mitchell, N.C., 1996. Creep in pelagic sediments and potential for morphologic dating of marine fault scarps. Geophys. Res. Lett. 23, 483 – 486.

Moore, G.F., Taylor, B., 1988. Structure of the Peru foerarc from multichannel seismic-reflection data. In: Suess E, von Huene R et al., Proc. ODP, Init Rept. 112, 71 – 76.

Müller, R.D., Roest, W.R., Royer, J.-Y., Gahagan, L.M., Sclater, J.G., 1997. Digital isochrones of the World's ocean floor. J. Geophys. Res. 102/2, 3211 – 3214.

Nash, D.B., 1981. FAULT: a FORTRAN program for modeling the degradation of active normal fault scarps. Comp. Geosci. 7, 249 – 266.

Norabuena, E., L. Leffler-Griffin, A. Mao, T. Dixon, S. Stein, I. S. Sacks, L. Ocola, and M. Ellis, Space geodetic observations of Nazca-South America convergence across the Central Andes, 1998. Science 279, 358-362.

Pecher, I.A., Kukowski, N., Hübscher, C., Greinert, J., Bialas, J., 2001. The link between bottom simulating reflections and methane flux into the hydrate stability zone – New evidence from Lima Basin, Peru Margin. Earth Planet. Sci. Lettr. 185, 343-354.

Pratson, L.F., Haxby, W.F., 1996. What is the slope of the U.S.continental slope ? Geology 24, 3 – 6.

Ramsay, L.A., Hovius, N., Lague, D., Liu, C.-S., 2006. Topographic characteristics of the submarine Taiwan orogen. J. Geophys. Res. 111, F02009, doi:1029/2005JF000314.

Ranero, C.R., von Huene, R., 2000. Subduction erosion along the Middle America convergent margin. Nature 404: 748 – 752.

Ranero, C.R., Villaseñor, A., Morgan, J.P., Weinrebe, W., 2005. Relationships between bend-faulting at trenches and intermediate-depth seismicity Geochemistry, Geophysics, Geosystems 12, doi:10.1029/2005GC000997.

Roberts, A., 2001. Curvature attributes and their application to 3D interpreted horizons. First Break 19/2, 85 – 100.

Rosenbaum, G., Giles, D., Saxon, M., Betts, P.G., Weinberg, R.F., Duboz, C., 2005. Subduction of the Nazca Ridge and the Inca Plateau: Insights into the formation of ore deposits in Peru. Earth Planet. Sci. Lett. 239, 18 – 32.

Sak, P.B., Fisher, D.M., Gardner, T.W., 2004. Effects of subducting seafloor roughness on upper plate vertical tectonism: Osa Peninsula, Costa Rica. Tectonics 23, TC1017, doi:10.1029/202TC001474.

Schildgen, T., Hodges, K.V., Whipple, K.X., Reiners, P.W., Pringle, M.S., 2007. Uplift of the western margin of the Andean plateau revealed from canyon incision history, southern Peru. Geology 35, 523 – 526, doi:10.1130/G23532A.1.

Schlunegger, F., Zeilinger, G., Kounov, A., Kober, F., Hüsser, B., 2006. Scale of relief growth in the forearc of the Andes of northern Chile (Arica latitude, 18°S). Terra Nova 18, 217 – 223.

Schweller, W.J., Kulm, L.D., Prince, R.A., 1981. Tectonics, structure and sedimentary framework of the Peru-Chile trench. In: Nazca Plate: Crustal Formation and Andean Convergence, Kulm, L.D. et al. (eds) Mem. Geol. Soc. Am. 154, 323 – 349.

Shary, P.A., Sharaya, L.S., Mitusov, A.V., 2002. Fundamental quantitative methods of land surface analysis Geoderma, 107, 1 – 32.

Somoza, R., 1998. Updated Nazca (Farallon)-South America relative motions during the last 40 Myr: Implications for mountain building in the central Andean region. J. South Am. Earth Sci. 11, 211 – 215.

von Huene, R., Bourgois, J., Miller, J., Pautot, G., 1989. A large tsunamigenic landslide and debris flow along the Peru trench. J. Geophys. Res. 94, 1703 – 1714.

von Huene, R., Lallemand, S.E., 1990. Tectonic erosion along the Japan and Peru convergent margins. Geol. Soc. Am. Bull. 102, 704 – 720.

von Huene, R., Gutscher, M.-A., Pecher, I.A., 1996. Development of the accretionary prism along Peru and material flux after subduction of Nazca Ridge. Tectonics 15, 19 – 33.

von Huene, R., Weinrebe, W., Heeren, F., 1999. Subduction erosion along the north Chile margin. J Geodynamics 27, 345 – 358.

von Huene, R., Ranero, C.R., 2003. Subduction erosion and basal friction along the sediment-starved convergent margin off Antofagasta. J. Geophys. Res. 108 (B2), 2079, doi:10.1029/2001JB001569.

Wessel, P., Smith, W.H.F., 1998. New, improved version of the Generic Mapping Tools released. EOS Trans. AGU 79 (47), 579.

Wright, D.J., Bloomer, S.H., McLeod, C.J., Taylor, B., Goodlife, A.M., 2000. Bathymetry of the Tonga trench and forearc: a map series. Mar. Geophys. Res. 21, 489 – 511.

Figure captions

Fig.1: Map displaying swath bathymetry recorded during the GEOPECO cruise and complemented with coverage from the SEAPERC cruise (Bourgois, 1990) with black boxes indicating SEAPERC data. Red lines are topographic profiles extracted from the swath data parallel to SO146 wide angle seismic profiles and shown in Fig.3. Blue lines refer to the age of the ocean floor (Mill. years, Müller et al., 1997). Lower left insets show the variation of convergence rate and obliquity at 12°S with time (Somoza, 1998). Red arrow indicates present direction and rate of convergence (Norabuena at el., 1998). Orange boxes refer to subsequent figures.

Fig.2: Morphology of the Nazca plate and trench region in corridors at **A** 9°S (off Yaquina basin, yellow dotted lines indicate crests of basalt ridges, white line indicates orientation of the trench), **B** 12°S (off northern Lima basin), and **C** 13.5° S (off southern Lima basin) matching the position of wide angle seismic profiles (Krabbenhöft et al., 2004). Outside the areas covered with swath data, bathymetry as obtained from the GINA data set (Lindquist et al., 2004) is displayed for regional information. For location, see Fig.1.

Fig.3: Bathymetry profiles along SO146 wide angle seismic profiles. Insets show the lower slope. For location see red lines in Fig.1.

Fig.4: Yaquina area. **A** Bathymetric map of the Nazca plate, the trench and continental slope. Numbers indicate palaeo-transform faults. **B** Perspective image, view from S, illumination from NE. For location, see Fig.1.

Fig.5: Mendaña region **A** Bathymetric map of the Mendana fracture zone, trench, and lower slope (merged SEAPERC (Bourgois et al., 1990) and GEOPECO data) **B** Perspective image, view from WWN, illumination from NE. For location, see Fig.1.

Fig.6 **A** Bathymetry seaward and landward of the trench in the Yaquina area **B** Local dip **C** Dip curvature. For location, see Fig.1.

Fig.7 **A** Bathymetry seaward and landward of the trench in the Mendana area **B** Local dip **C** Dip curvature. For location, see Fig.1.

Fig.8: Histograms showing the frequency distribution of local slopes (same areas and data sets as in Figures 6 and 7. **upper** Yaquina area, left: Nazca plate seaward of the trench; right: continental slope landward of the trench **lower** Mendaña area, left: Nazca plate seaward of the trench; right: continental slope landward of the trench.

Fig.9: **A** large scale map of gullies at upper slope. For location, see Fig.4. **B** topographic profiles along the slope. For location, see **A.**

Fig.10: Lima Region: Bathymetric map of the mid and upper slope revealing a channel system originating from distributed drainage, a half-moon shaped tip of a slump scar and the slump mass. White box indicates area shown in Fig.11b.

Fig.11: Morphometric dating of slumps: **A** Bathymetry of the Paita slump, **B** bathymetry of the Lima slump. In both pictures, positions of profiles across the slump and along the slump scar are indicated **C** Profiles across the Paita slump **D** Profiles across the Lima slump. Western and southern ends of the profiles were assigned to "0" on the ordinate. For location of the Lima map, see Fig.10.

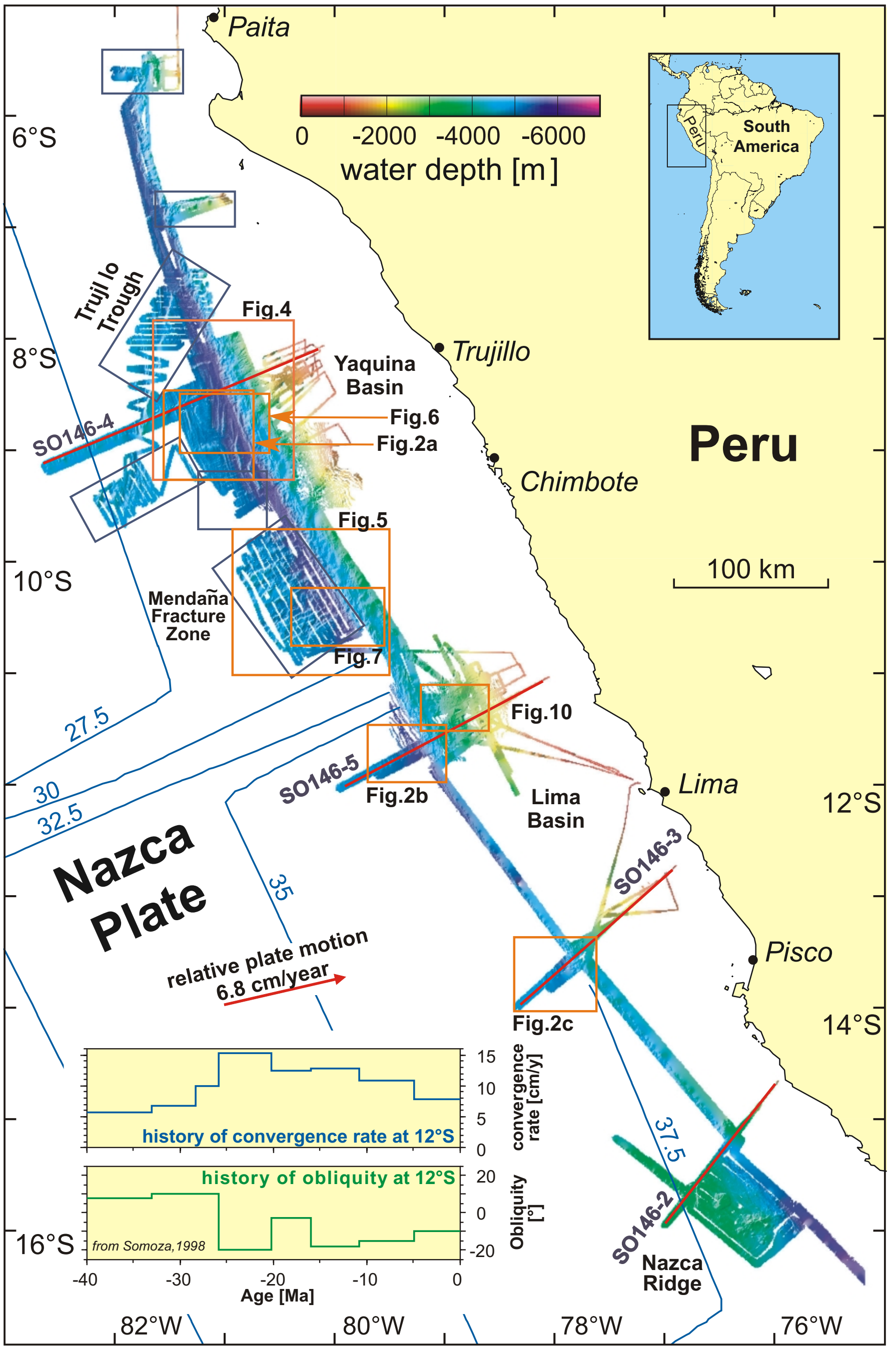

Kukowski et al., MARGO 2008; doi:10.1017/j.margeo.2008.05.017Fig.1

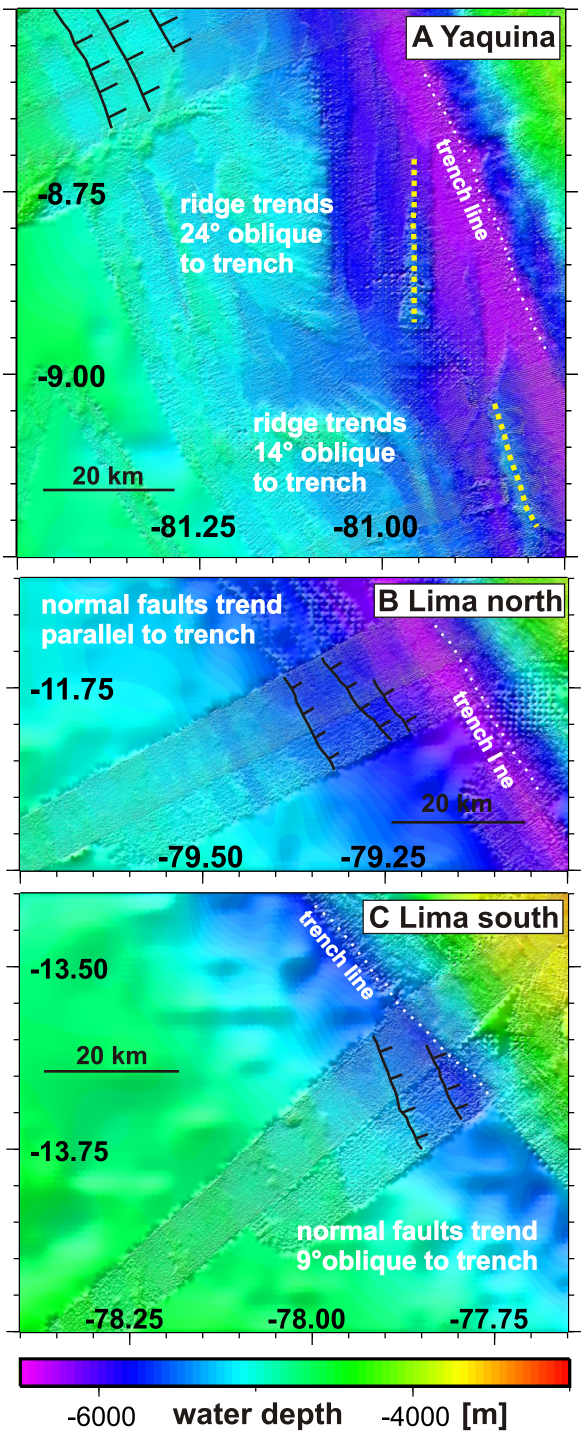

Kukowski et al., MARGO 2008; doi:10.1017/j.margeo.2008.05.017Fig.2

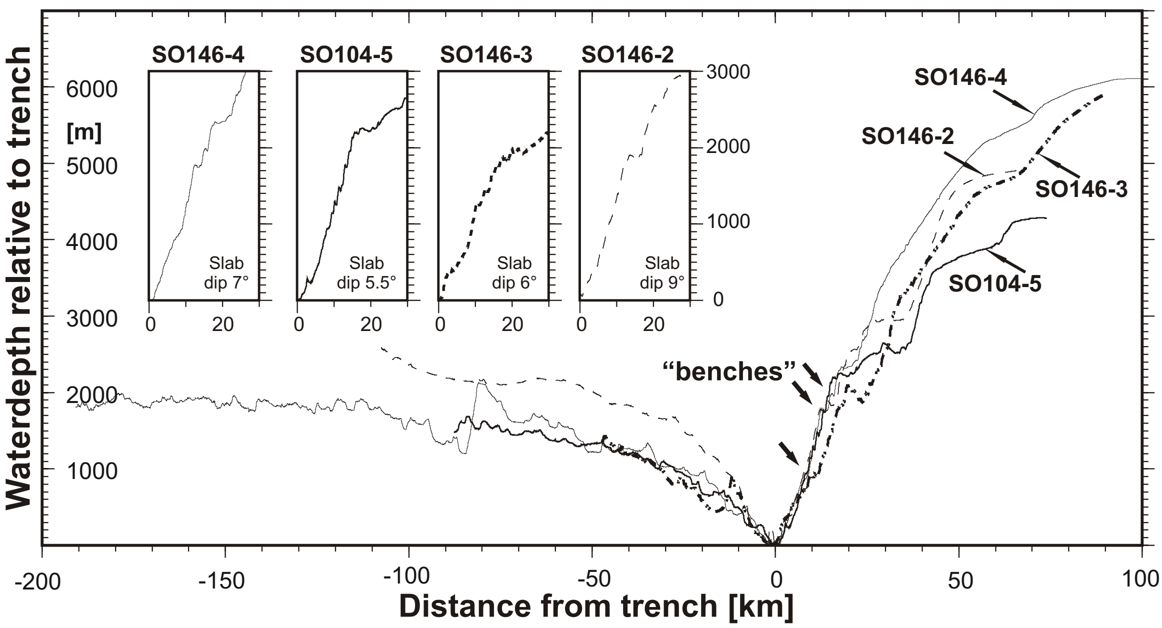

Kukowski et al., MARGO 2008; doi:10.1017/j.margeo.2008.05.017Fig.3

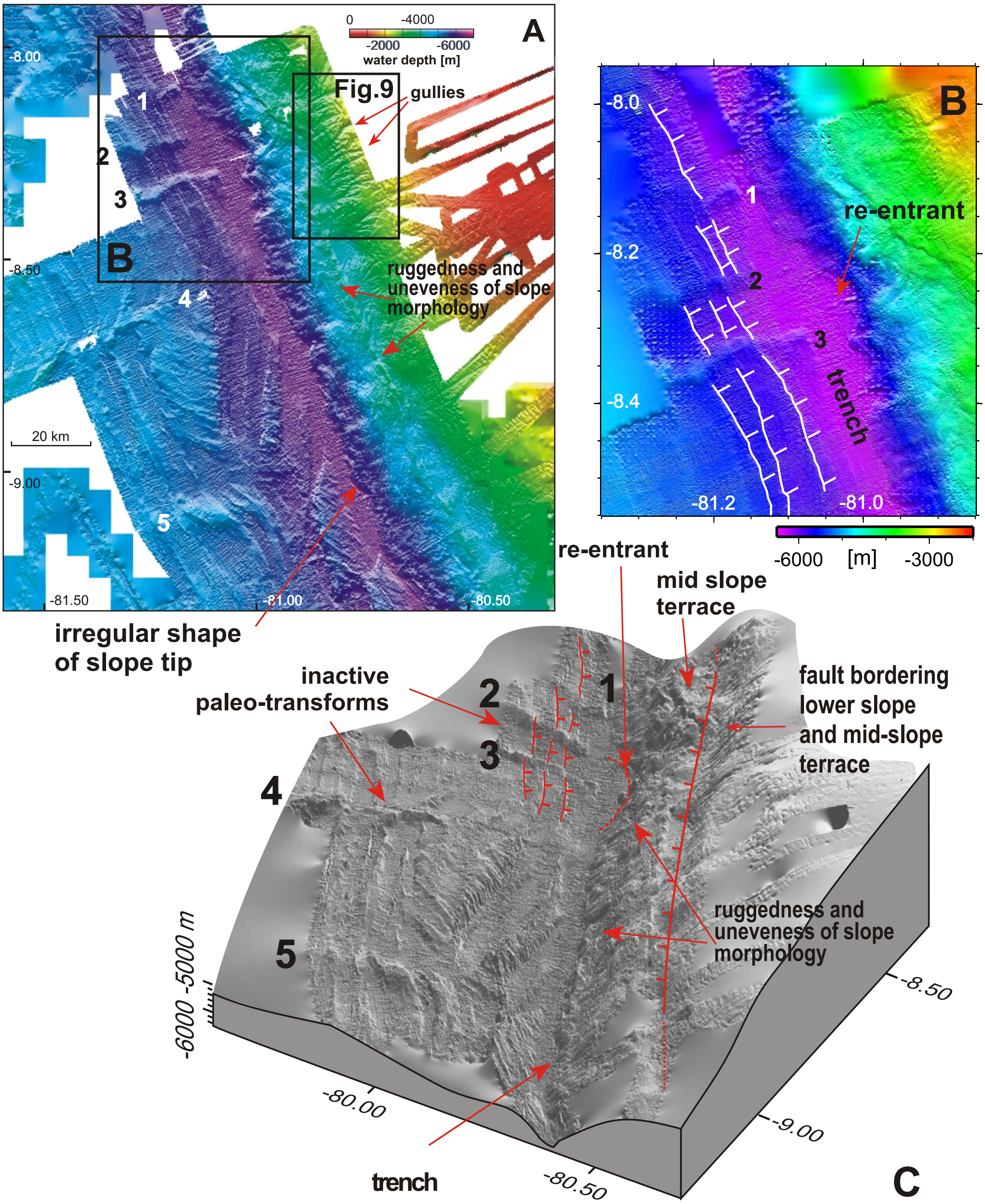

Kukowski et al., MARGO 2008; doi:10.1017/j.margeo.2008.05.017Fig.4

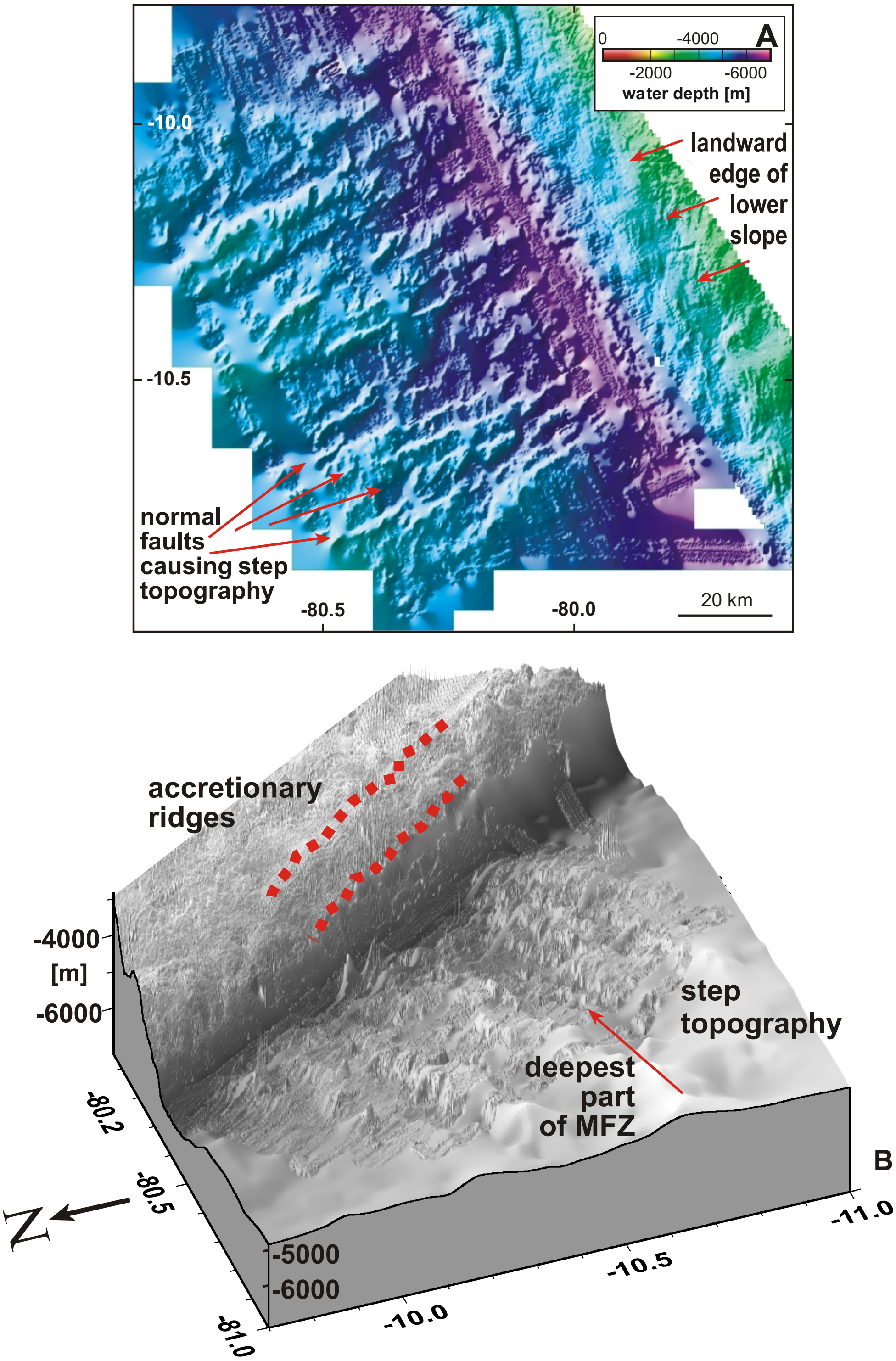

Kukowski et al., MARGO 2008; doi:10.1017/j.margeo.2008.05.017Fig.5

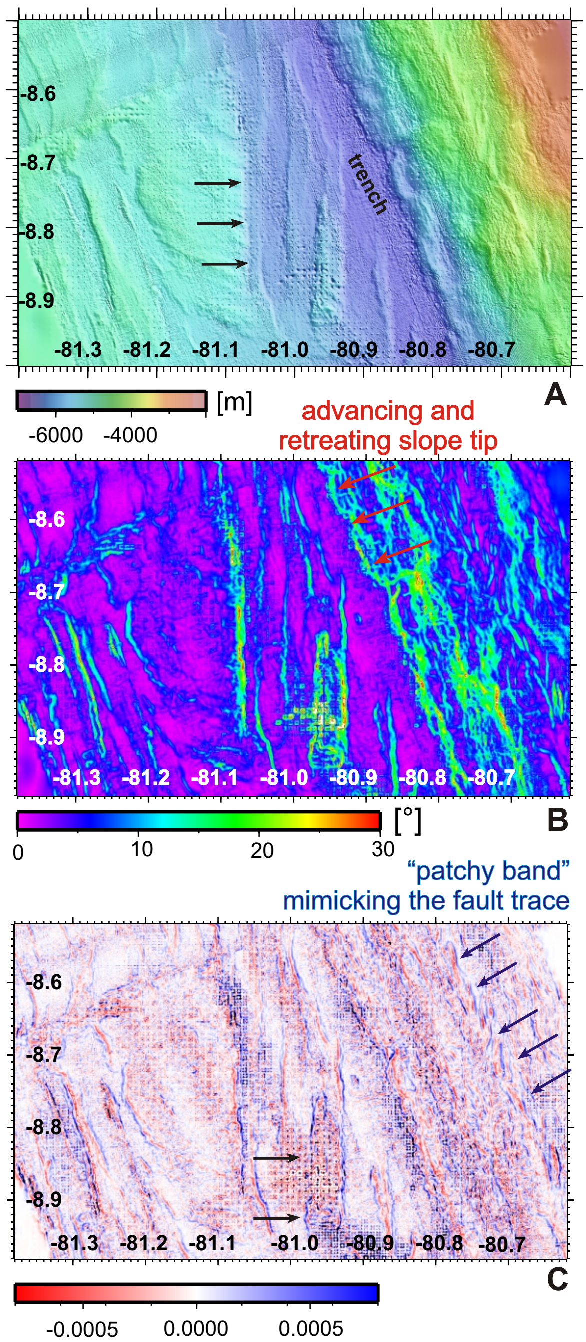

Kukowski et al., MARGO 2008; doi:10.1017/j.margeo.2008.05.017Fig.6

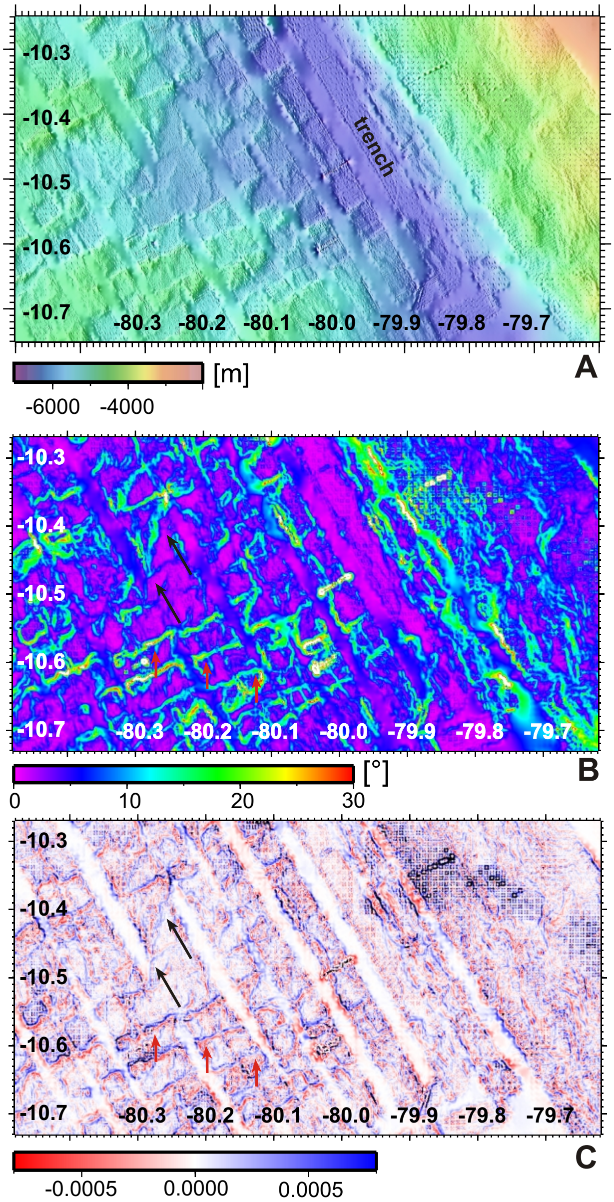

Kukowski et al., MARGO 2008; doi:10.1017/j.margeo.2008.05.017Fig.7

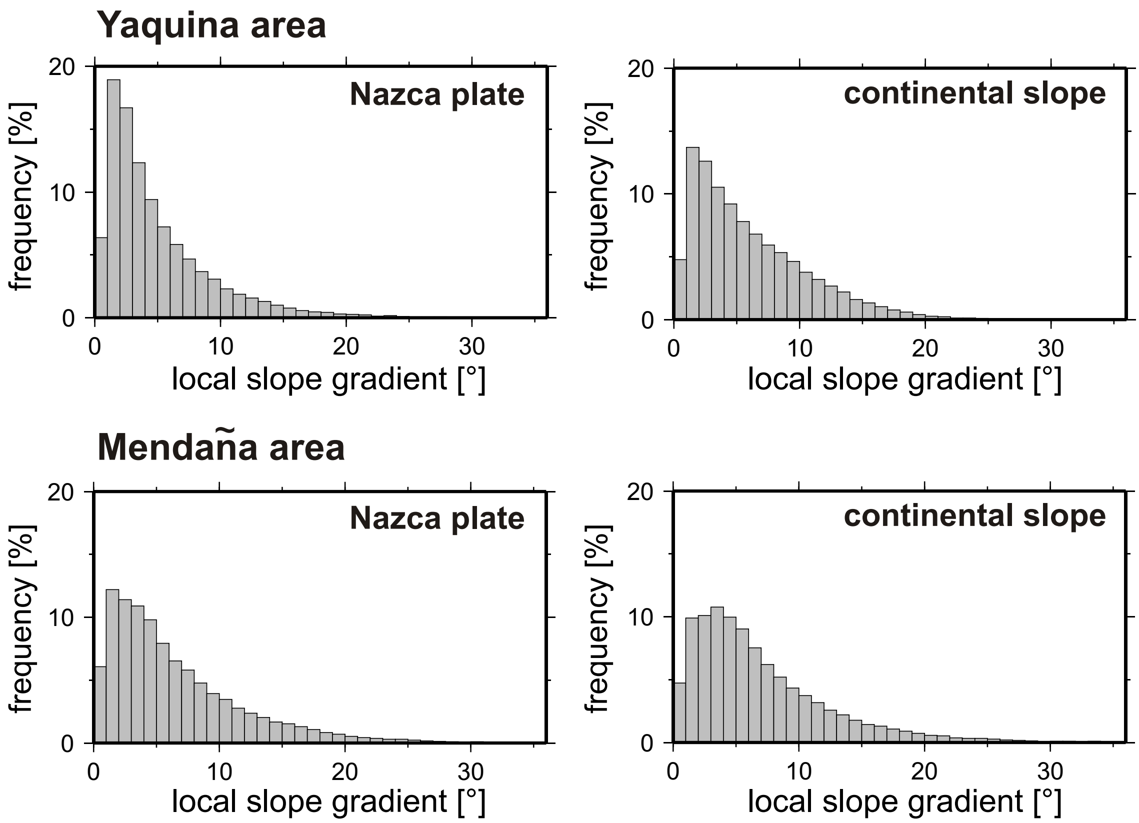

Kukowski et al., MARGO 2008; doi:10.1017/j.margeo.2008.05.017Fig.8

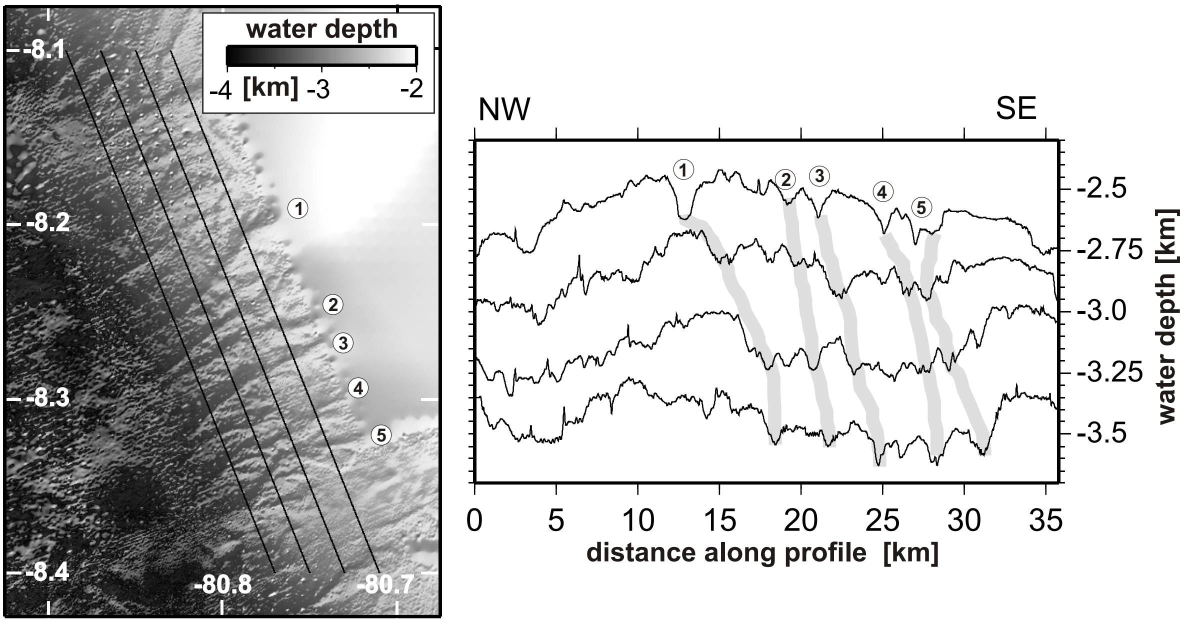

Kukowski et al., MARGO 2008; doi:10.1017/j.margeo.2008.05.017Fig.9

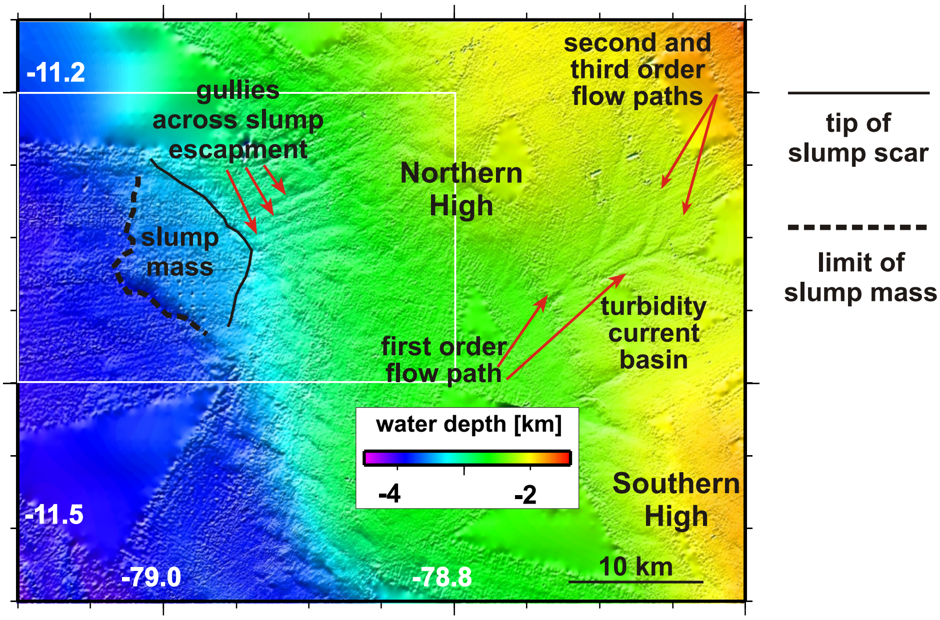

Kukowski et al., MARGO 2008; doi:10.1017/j.margeo.2008.05.017Fig.10

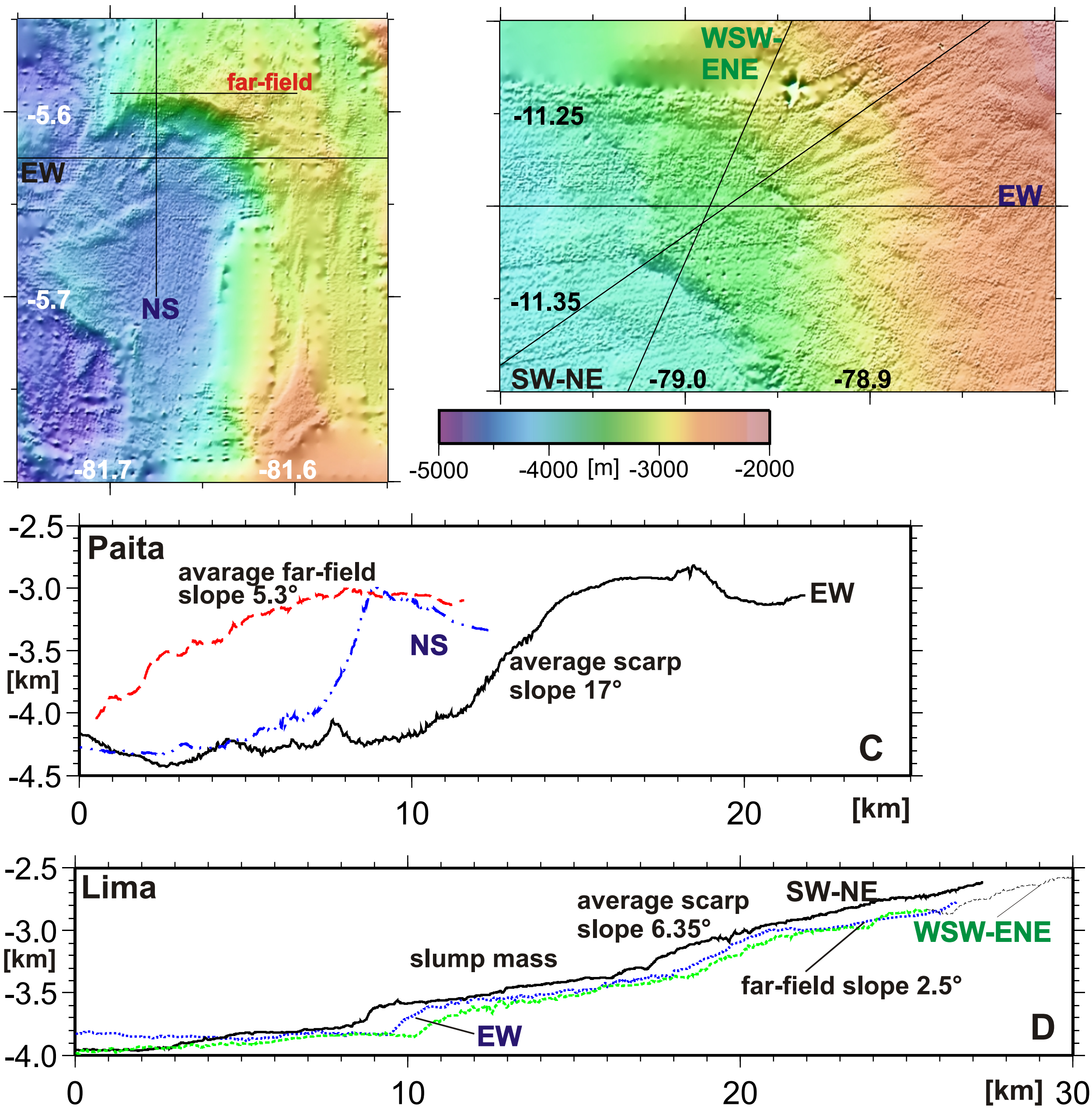

Kukowski et al., MARGO 2008; doi:10.1017/j.margeo.2008.05.017Fig.11